



Available online at
ScienceDirect
www.sciencedirect.com

Elsevier Masson France
EM|consulte
www.em-consulte.com/en



Original article

X-ray and optical spectroscopic study of the coloration of red glass used in 19th century decorative mosaics at the Temple of the Emerald Buddha

Bruce Ravel^{a,*}, G.L. Carr^b, Christoph A. Hauzenberger^c, Wantana Klysubun^d

^a National Institute of Standards and Technology, Gaithersburg, MD 20899, USA

^b Photon Sciences, Brookhaven National Laboratory, Upton, NY 11973, USA

^c Karl-Franzens-Universität Graz, Graz 8010, Austria

^d Synchrotron Light Research Institute, Nakhon Ratchasima 30000, Thailand

ARTICLE INFO

Article history:

Received 30 December 2013

Accepted 4 June 2014

Available online xxx

Keywords:

XAFS

Colloidal gold

Decorative glass

ABSTRACT

The Temple of the Emerald Buddha in Bangkok, Thailand is noted for its glass mosaic decorations on exterior walls and statuary. The original mosaic artwork dates to the early 19th century and is composed of variously-colored, mirrored glass pieces. In this work, we examine the chemical composition and optical properties of the red glass manufactured at that time. Through the use of X-ray and optical spectroscopies, we demonstrate evidence that the 19th century craftsmen produced “ruby-gold” glass, wherein the red coloration is caused by the dispersal of nanoscale metallic gold particles throughout the glass matrix.

Published by Elsevier Masson SAS.

1. Introduction

Built in 1782, the Temple of the Emerald Buddha is the largest Buddhist temple in Bangkok, Thailand. During the reign of King Rama III (1824 to 1851), the temple was restored as additional halls, pagodas and towers were constructed. The temple renovation included the use of mosaics composed of thin, mirrored glass in place of the more traditional gold-on-red lacquer art to decorate external walls and pillars of the Ordination Hall enshrining the Emerald Buddha [1,2]. These decorative glasses, commonly called Kriab mirrors, are leaded glass containing from 10% to 50% lead by weight (see Table 1 and reference [3]). They were fabricated in glasshouses sponsored [4] by Thai royalty. They are thin (300 μm to 1000 μm), translucent, and variously-colored. Glass of all colors was coated with a reflective metal paste on their back surface and affixed to exterior surfaces of the Ordination Hall using natural latex.

The royal Glass Department Production was terminated during the reign of King Rama V (1868 to 1910). Thus, the Kriab glass has not been produced in Thailand in over 100 years. Scant records of the glass-making techniques remain. Eight manuscripts National Library of Thailand [5] titled in Thai as “Textbook of glass melting” belonged to Prince Pramoch, the Head of Glass Production

Department of King Rama IV, and were later donated to the National Library of Thailand in 1915. The language in these records is archaic and difficult for the modern reader. Some information on glass fabrication can be interpreted from these sources [6], such as a list of raw materials which includes, tin, saltpeter, gold, lead, red soil, bronze, white stone powder and coloring glazes. No details of the manufacturing process remain which are known to us.

Over decades and with exposure to 20th century air pollution, the adhesion of the glass pieces to the walls degraded. By the time of the latest restoration of the Temple, beginning in 1982, the integrity of the mosaics was compromised by the loss of significant numbers of glass pieces. Without ready means of reproducing glass in the original style, commercially-sourced glass mirrors were imported and used in restorations beginning in 1982. The modern and original glasses have several aesthetic differences, as shown in Fig. 1. The modern glass is thicker, differently colored, and more reflective than the original glasses. The conservators of the Temple are interested in future restoration to more closely resemble the original visual appearance. Scientists at the Synchrotron Light Research Institute, Thailand’s national synchrotron user facility, were asked to investigate [3] the composition of original Kriab mirror pieces from the Ordination Hall.

In this paper, we examine original specimens of red-colored glass from the Temple. The physical mechanism by which small, spherical, metal inclusions drive the coloration of glass has been understood for over a century [7,8] with dispersed gold resulting in a red coloration. Some extant historical glasses are colored red by

* Corresponding author. Tel.: +1631 344 3613; fax: +1 631 344 5419.
E-mail address: bravel@bnl.gov (B. Ravel).

Table 1
Major elements determined by EDX-WDX SEM [mass fractions, expressed as percentages, as oxides]. Uncertainties are discussed in the text.

	KMHR1	KMSR2	KMHCL2
SiO ₂	37.99 (9)	37.59 (77)	68.42 (42)
TiO ₂	<0.15	<0.15	<0.15
Al ₂ O ₃	1.41 (9)	1.20 (13)	1.71 (8)
Fe ₂ O ₃	0.37 (5)	0.31 (4)	1.37 (7)
MnO	<0.15	<0.15	1.01 (5)
MgO	0.53 (12)	0.56 (11)	0.65 (15)
PbO	46.33 (103)	51.77 (124)	1.27 (3)
CaO	0.94 (4)	0.90 (8)	8.45 (7)
Na ₂ O	3.86 (5)	3.86 (14)	12.96 (28)
K ₂ O	0.78 (1)	0.81 (3)	1.09 (2)
Sum	92.20 (103)	97.01 (131)	96.92 (31)

the presence of dispersed, nanoscale gold and called “ruby-gold” glass. The most famous example is the Lycurgus Cup, a Roman artifact dating from the fourth century C.E. [9] which is a brilliant red when seen under transmitted light. Lost in Europe during the middle ages, this coloration technique remained used throughout the Arab world during that period [10]. It was rediscovered and widely used in Europe beginning in the seventeenth century [10,11]. Small gold particles can be dispersed in glass by adding either hydrous chloroauric acid (HAuCl₄ × H₂O) or potassium aurocyanide (KAu(CN)₂) to the molten glass followed by a reducing agent such as SnO₂, along with control of redox conditions as the glass is annealed [12]. The reducing agent serves as an electron source, reducing the gold to its zero-valent state. As the glass cools and anneals, spherical inclusions with diameters in the range of 20 nm to 100 nm are dispersed throughout the glass. This mechanism has been inferred [13] as the source of the red coloration of similar period glasses from Thailand on the basis of the presence of gold in proton-induced x-ray emission (PIXE) spectra, but has not been demonstrated quantitatively.

Haslbeck et al. [12] explain how a reducing agent such as SnO₂ added to a glass melt along with a gold salt can act as an electron source, reducing the gold to the metallic nanoparticles responsible for red coloration. To test the conjecture that mid-nineteenth century Thai craftsmen may have used a similar technique to make red glass, we have performed a chemical analysis using wavelength and energy dispersive X-ray spectroscopy (WDX/EDX) and laser ablation inductively coupled plasma mass spectrometry (LA-ICP-MS) to determine concentrations of major, minor, and trace elements in the glasses. We then applied X-ray and optical spectroscopy methods to characterize the gold content of our red glass samples.

**Fig. 1.** Original Kriab glass mosaic on a piece of concrete wall on display in the Museum of the Temple of the Emerald Buddha. (Inset) Examples of modern, commercial glass used in 20th century restorations.

In this paper, we demonstrate that gold is present in these red glass specimens in a metallic form and in a size and concentration known to produce red coloration. We discuss other possible coloration mechanisms, but conclude that gold is the principle coloring agent of these glasses.

2. Experimental methods

The glass samples studied here were obtained from the Thailand Bureau of the Royal Household [4] and come from different locations around the Temple. Sample KMHR1 was a hexagonal piece originally from one of eight inner pillars of the Ordination Hall and part of a pattern like the one shown on the left of Fig. 1. It was removed from the pillar at the time of a restoration effort in 1982. The piece measured by X-ray and optical spectroscopy is one of three pieces cut from the hexagon and used for different analyses. It is about 5 mm by 12 mm and 600 μm thick. Sample KMSR2 was removed a mosaic pattern like the one shown in Fig. 1 decorating a damaged piece of a concrete wall and housed in the Museum of the Temple of the Emerald Buddha. It is approximately square, about 8 mm on a side, and 960 μm thick. Both samples were cleaned with ethanol prior to X-ray and optical measurements. The samples are shown in the inset to Fig. 3.

Both pieces have weathered surfaces on the sides shown in Fig. 3 and both pieces are partially covered on the reverse side by the oxidized remains of the tin-lead alloy used to make the reflective Kriab mirrors. Both pieces have sharp edges indicative of having been formed into mosaic pieces by scoring and breaking, rather than by cutting while in a hot, softened state. Finally, both pieces are uniformly colored throughout their bulk.

X-ray Absorption Spectroscopy (XAS) data at the gold L_{III} edge (11919 eV) were measured at beamline X23A2 at the National Synchrotron Light Source at Brookhaven National Laboratory in New York, USA. This is an unfocused bend magnet beamline using a Si(311) monochromator of a fixed-exit, Golovchenko-Cowan [14] design. Harmonic rejection is made by a single bounce, flat, Rh-coated mirror. An argon-filled ionization chamber was used as described below to measure the intensity of the incident beam, which was about 10⁹ photons per second in a spot of 1.5 mm in the horizontal and 0.5 mm in the vertical. At this low flux density, radiation induced changes in speciation are rarely observed, even in hydrated samples. No such changes were observed in the data presented here or in any other XAS measurements made on the Kriab glasses. A four-element, Si-drift, energy-discriminating detector was used to measure the X-ray fluorescence intensities. All fluorescence XAS spectra were corrected for dead-time using the algorithm of Woicik et al. [22].

Because the glass pieces have very low concentrations of gold, the XAS data were measured in the fluorescence geometry. The glass pieces are, however, too thick to allow transmission of the beam at the energy of the Au L_{III} edge for the purpose of measuring a reference for energy calibration. Given the large number of scans measured on each sample and the relatively poor angular repeatability of the monochromator, measurement of an energy calibration reference is essential. To do this, we replaced the standard ionization chamber used to measure the incident intensity, *I*₀, with the argon-filled, four-channel, ionization chamber described by Ravel et al. [15]. This is shown schematically in Fig. 2. Using the same slit assembly described in that paper to define the multiple incident beams, the two central channels were blocked at the slit assembly using lead tape. This left the inboard and outboard beams, which are separated by 14 mm, for use in the experiment. The sample was placed in the path of the outboard beam, which was used to measure the fluorescence. The inboard beam passed beside the glass sample unimpeded, then struck a gold foil through

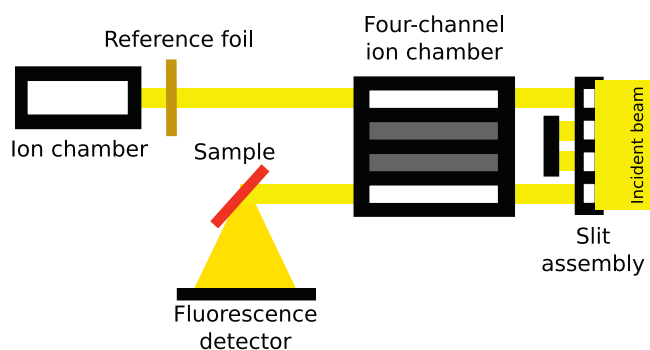


Fig. 2. A schematic of the experimental arrangement for the XAS measurements. The unfocused bend magnet beam fully illuminates the 22 mm wide slit assembly. The middle two channels are blocked, while X-rays enter the outer channels of the four-channel ionization chamber [15]. These two signals have independent signal chains and are used as I_0 for the sample and the reference, respectively. The two beams then strike the glass sample and reference foil simultaneously.

which transmission XAS was measured using a standard nitrogen-filled ionization chamber. This foil spectrum was used as the energy reference. The incidence and measurement signals for the fluorescence and reference samples were thus measured independently and simultaneously.

The low gold concentrations required many repetitions of the XAS scans on each sample. Forty-two scans were made on sample KMHR1, while thirty scans were made on sample KMSR2. The raw data were processed, aligned, and calibrated against the reference measurements using the Athena program [16]. The difference spectrum analysis described in Sec. 4 was also performed using this program.

Cu K-edge (8979 eV) XAS spectra of the red glasses were acquired in fluorescence mode at the beamline BL8 [17] of the Synchrotron Light Research Institute in Nakhon Ratchasima, Thailand. The incident beam is unfocused, monochromated by Ge(220) double crystals, 10 mm in the horizontal and 1 mm in the vertical with flux of about 10^9 photons per second. The incident beam intensity was measured by an ionization chamber filled with a mixture of nitrogen and helium gases. The fluorescence signal was measured using a 13-element germanium energy-discriminating detector and corrected for dead time. The samples were in air during the measurements. A Cu foil was used for energy calibration. Copper (I) oxide and copper (II) oxide were used as references for copper speciation. A colorless glass (KMHCL2) of the same era was collected from the same pillar as the sample KMHR1 was also measured at the Cu K-edge. XAS spectra from the glass samples were averaged from 6 to 10 scans.

Optical transmission measurements were performed using synchrotron light at beamline U10 of the National Synchrotron Light Source. A Bruker Vertex 80v Fourier transform spectrometer¹ equipped with a UV-visible CaF₂ beam-splitter was used in combination with both GaP and Si photodiode detectors to span photon energy ranges from about 1 eV up to 3.5 eV. One surface of the glass samples had the oxidized remnants of the metal used to mirror the glass. This material blocked some of the light passing through the sample, but did not show any specific features in the visible spectral region.

¹ Certain commercial materials are identified in this paper to foster understanding. Such identification does not imply recommendation or endorsement by the National Institute of Standards and Technology, nor does it imply that the materials or equipment identified are necessarily the best available for the purpose.

Table 2

Minor and trace elements determined by LA-ICP-MS [mg/kg]. Uncertainties are discussed in the text.

	KMHR1	KMSR2	KMHCL2
Ti	212(5)	182(11)	377(5)
Mn	416(8)	309(19)	7594(70)
Cu	2204(36)	1883(58)	281(1)
Zn	82(2)	78(4)	436(3)
As	3234(35)	3616(50)	567(11)
Rb	56(2)	50(2)	26(1)
Sr	21(1)	18(1)	105(1)
Zr	20(1)	16(1)	53(1)
Ag	14(1)	13(1)	61(2)
Sn	77(3)	59(3)	169(1)
Sb	60(1)	56(3)	730(24)
Ba	91(1)	82(6)	708(16)
Au	45(1)	49(2)	

3. Chemical analysis

Small pieces of KMHR1, KMSR2, and KMHCL2 were cut and mounted in the two component resin Technovit 5071 (Heraeus Kulzer GmbH) for chemical analysis. The resin mounted sample was polished and cleaned in an ultrasonic bath of de-ionized water. Possible surface contamination can be excluded since the first few seconds from the laser ablation signal, where the surface is ablated, is excluded by default from quantification.

Concentration of major elements expressed as simple oxides, including SiO₂, TiO₂, Al₂O₃, Fe₂O₃, MnO, MgO, CaO, PbO, Na₂O, and K₂O, were determined by a JEOL 6310 scanning electron microscope equipped with an Oxford EDX and a Microspec WDX spectrometer at the Institute of Earth Sciences, University of Graz, Austria. These results are shown in Table 1. Samples were coated with carbon and a conductive film was used to make electrical contact with the aluminum sample holder. Analytical conditions were set to 15 kV accelerating high voltage and a sample current of 6 nA. A defocused beam (about 6 μm x 10 μm spot size) was used to minimize loss of volatile elements such as sodium. Lead and sodium were analysed by the WDX spectrometer, which has a typical mass fraction detection limit of 0.05. All other elements, shown in Table 2, were analysed by the EDX spectrometer with a mass fraction detection limit of 0.1 to 0.15. Natural mineral standards and the BCR-2G glass from the USGS [18] were used for standardization: Si (BCR-2G), Ti, Ca (titanite), Al, K (adularia), Fe (BCR-2G), Mn (rhodonite), Mg (BCR-2G), Na (jadeite), Pb (galena). The BCR-2G reference material was analysed for quality control at the beginning, in the middle and at the end of the measurements of the glass samples. Major elements could be reproduced within certified values. Sulfur, chlorine and phosphorus contents were verified qualitatively by the EDX spectrometer, but no significant amounts were detected. The light elements, Li, Be, and B, cannot be detected using the EDX spectrometer and so were analysed by LA-ICP-MS. No significant amounts were detected. The totals of the constituents do not sum up to mass fraction 100%. The low totals are likely related to H₂O content in the glass or to a loss of Na during analyses despite the low current and defocused beam that were used. The uncertainties of the oxide concentrations were determined from the standard deviation of 3 to 4 measurements at different spots on the sample.

Trace element concentration of the glasses was analyzed with a LA-ICP-MS system (Laser ablation unit: ESI NWR 193; ICP-MS: Agilent 7500) at the Central Lab for Water, Minerals and Rocks, NAWI Graz, Karl-Franzens-University Graz and Graz University of Technology, Austria. The material was ablated by using a 193 nm laser pulsed at 9 Hz, 75 μm spot size with an energy of 6.5 J/cm². Helium was used as carrier gas at 0.8 L/min flow and data were acquired in time resolved mode. For each analysis, a gas blank was obtained for background correction. The laser was active for 60 seconds followed

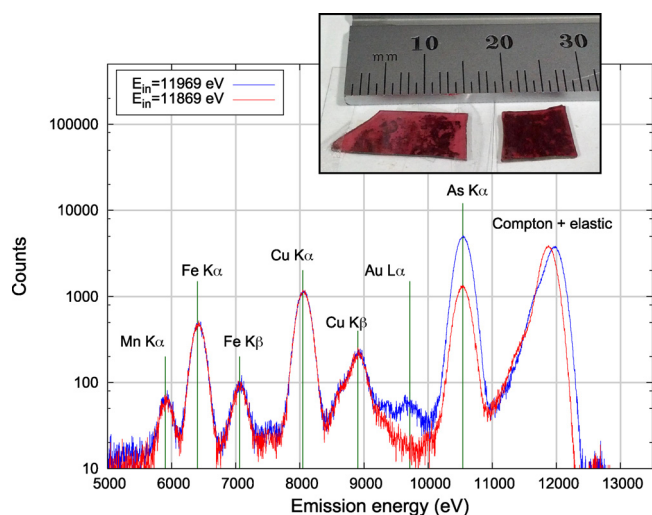


Fig. 3. X-ray fluorescence spectra for sample KMHR1 measured with incident beam energy of ± 50 relative to the Au L_{III} edge (11919 eV), thus emphasizing the Au $L\alpha$ peak at 9713 eV. (Inset) Photograph of the two red glass samples: KMHR1 is on the left, KMSR2 is on the right. The dark regions are oxidized metal on the backside showing through the translucent glass.

by 50 seconds washout time. The standard glass NIST610 [19] was routinely analyzed for standardization and drift correction while standards NIST612 [19], NIST614 and BCR-2 [20] were analyzed as unknowns to monitor the accuracy of the measurements. All standards could be reproduced within $\pm 10\%$ of the certified values [19,20]. Silicon was used as an internal standard. The uncertainty of the oxide concentration was determined from the standard deviation of 3 to 5 measurements at different spots on the sample.

4. Spectroscopic results

4.1. Au L_{III} edge XAS

The X-ray fluorescence spectrum measured from sample KMHR1 is shown in Fig. 3. The XRF spectrum of sample KMSR2 is substantively identical. Along with various trace transition metals commonly found [3] in these glasses, we find a substantial amount of arsenic and a trace quantity of gold. Arsenic is a common contaminant [21] in natural galena (lead sulfide, PbS), a possible source for the lead found in abundance in these glasses. (Lead is not seen in Fig. 3, which shows measurements with the incident beam below the Pb L_{III} edge energy of 13035 eV.) The presence of As is a complicating factor in these measurements. The As K-edge is 11867 eV, only 52 eV below the Au L_{III} edge at 11919 eV. As a result, every XAS scan through the Au L_{III} edge passes through the As K-edge as well. The Au $L\alpha$ and As $K\alpha$ lines are separated by 800 eV, however the energy resolution of the detector [22] is about 250 eV when run with a 100 microsecond shaping time to minimize pile-up in the measured signal. With this energy resolution and the abundance of As relative to Au, the tail of the As $K\alpha$ peak contributes significantly to the spectral weight in the energy range of the Au $L\alpha$ line. The Cu $K\beta$ peak at 8904 eV is also present. While this is a similar separation from the Au $L\alpha$ peak at 9713 as the As $K\alpha$ peak at 10543 eV, the Cu signal is not changing during the measurement, thus is only a constant contribution to the background.

The extent of the contamination of the Au XAS spectrum by the much larger quantity of As in these glasses is seen in the top panel of Fig. 4. The principle step in these data occurs at the position of the As K-edge. In the second panel, these data are treated as As K-edge data for the purpose of normalization and are shown along with As

K-edge data from the same sample measured properly – i.e. with the discriminator window of the detector set around the As $K\alpha$ peak.

The same As white line is measured in both spectra. However, excess spectral intensity is observed above the Au L_{III} edge in the spectrum measured with the discriminator window around the Au $L\alpha$ peak. The problem, then, is to extract an interpretable Au signal from these data.

A difference spectrum is computed by subtracting the properly measured As K-edge data from the current spectrum. This is shown in the third panel of Fig. 4. The resulting difference spectrum shows a distinct jump at 11919 eV, the energy of the Au L_{III} edge. The spurious point at 11878 eV is an artifact of interpolation. The As K-edge data used to make the difference spectrum were measured on a fine energy grid through the edge and white line while the energy grid of the Au L_{III} measurement was much more sparse in that energy range.

The difference spectrum is treated as a XAS spectrum. The result of this normalization is shown in the bottom panel along with a XAS spectrum measured on a gold foil in transmission. While the extraction is unreliable above 12000 eV, the difference spectrum is clearly dominated by the XAS signal from metallic gold. The XAS spectra of bulk and colloidal gold [23] are known to be nearly identical. Performing the same analysis on sample KMSR2 resulted in a difference spectrum likewise dominated by the XAS signal from metallic gold.

4.2. Cu K-edge XAS

Red glass can also be colored by copper [24,25] or by selenium [26], both of which are common red colorants in contemporary glass. While the glasses studies here have copper in much higher concentration than gold, selenium is not present within the ~ 1 mg/kg detection limits of the LA-ICP-MS and X-ray fluorescence spectroscopy presented.

Copper offers two plausible mechanisms for the red coloration of these glasses. Cuprite, monovalent Cu_2O , is a brilliant red crystal with coloration controlled by optical absorption arising from transfer of charge from the O^{2-} anion to the Cu^{1+} cation. [27] Copper, like gold, has an optical response leading to a lustrous, yellowish color in the bulk metal. Like gold, it can act as a red colorant when present in glass as dispersed sub-100 nm metallic particles.

Cu K-edge (8979 eV) XAS spectra of the red glasses and the copper standards are shown in Fig. 5. The glass samples show the prominent peak at about 8983 eV corresponding to an electronic transition from 1s to 4p [28] characteristic of monovalent Cu_2O . The copper in these glasses is clearly monovalent, like cuprite. However, monovalent copper in the glass has a filled d -band which precludes charge transfer and therefore precludes optical absorption [27]. That the colorless glass contains Cu in the same chemical state, albeit in lower concentration [3], as the red glass indicates that the Cu^{1+} species does not contribute to the coloration.

The glass samples show no evidence of metallic content in their XAS spectra. However, the same is true of Cu XAS measured on copper-ruby glasses, as discussed by Nakai et al. [33]. In that work, the authors concluded that the red coloration is due to dispersion of less than 5% of the Cu content as a metallic colloid, while the rest is the same non-color-forming Cu^{1+} species that we observe here. To understand the roles of Au and Cu in the coloration of these glasses, we examine their optical spectrum.

4.3. Optical spectroscopy

Optical spectroscopy further confirms the identification of metallic gold particles dispersed throughout the glass and explains the red color of these samples. Fig. 6 shows the optical absorbance spectrum A of sample KMHR1, which is related to the measured

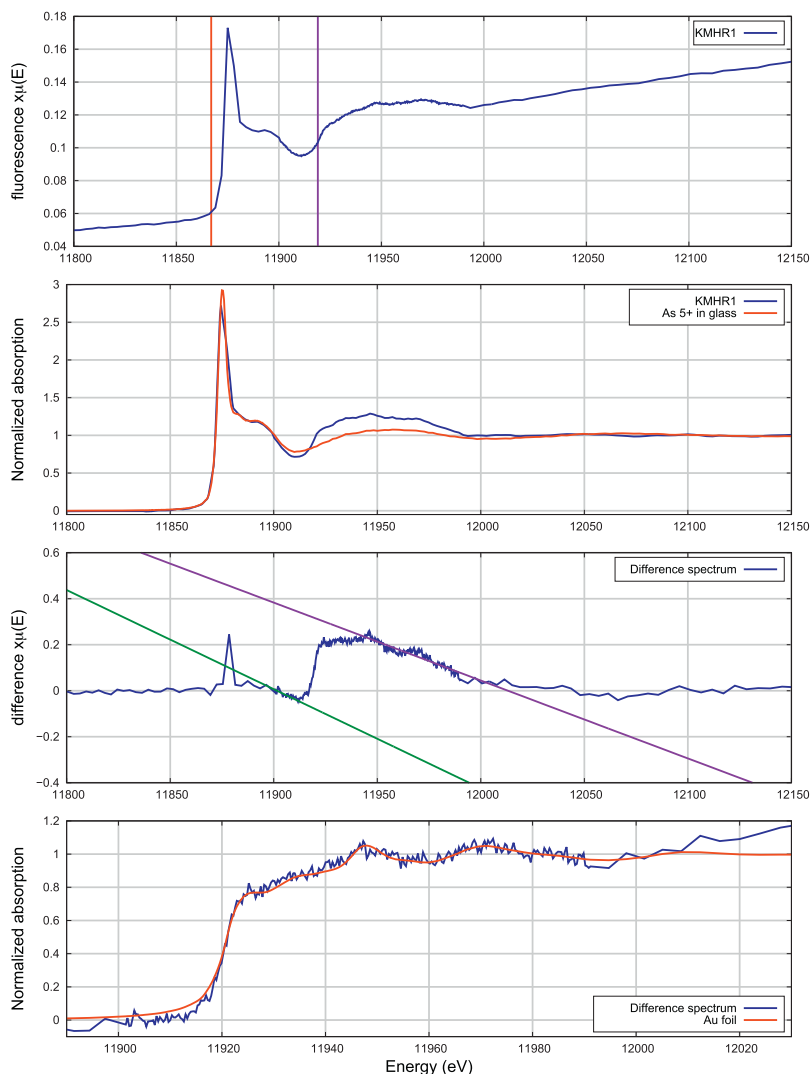


Fig. 4. (Top) The average of 42 XAS spectra measured at the Au L_{III} edge on sample KMHR1. The red vertical line marks the tabulated As K-edge energy at 11867 eV. The violet vertical line marks the tabulated Au L_{III} edge energy at 11919 eV. (Second) Comparison of these data to As K-edge data measured from the same sample. (Third) The difference spectrum obtained by subtracting the properly measured As K-edge spectrum from the Au L_{III} edge data. Also shown are the pre- and post-edge lines used in the edge-step normalization of the data. (Bottom) The normalized difference spectrum compared with XAS measured in transmission on a gold foil.

transmission T by $A = -\log_{10}(T)$. The absorbance of sample KMSR2 was essentially identical, except for an overall lower optical transmission due to more residual opaque adhesive on the back side.

The absorption spectrum of Fig. 6 is typical of small (<100 nm diameter), spherical, metallic gold particles embedded in a host matrix of glass [30]. This general behavior was first explained by the effective medium theory of J.C.M. Garnett [7,8]. Garnett was specifically interested in explaining how various metals in glass produced distinct colors. His theory for the effective optical response ϵ_{eff} of a composite material consisting of spherical particles with dielectric response ϵ_a embedded in a host material having dielectric response ϵ_b takes the form [31]:

$$\epsilon_{eff} = \epsilon_b + \epsilon_b \frac{3f(\epsilon_a - \epsilon_b)}{(1-f)(\epsilon_a - \epsilon_b) + 3\epsilon_b}, \quad (1)$$

where f is the volume fraction occupied by the spherical particle inclusion. In the case of colored glass materials, the volume fraction of metal particles is typically less than 0.1%. In the limit of small f , the average response can be approximated as:

$$\epsilon_{eff} = \epsilon_b + \epsilon_b \frac{3f(\epsilon_a - \epsilon_b)}{\epsilon_a + 2\epsilon_b}, \quad (2)$$

indicating a resonance condition can exist when $\epsilon_a = -2\epsilon_b$. From this effective dielectric response, one can calculate the complex refractive index $n \equiv \eta + i\kappa = \epsilon^{1/2}$ from which standard optical quantities such as the reflectance and absorption can be determined.

A consequence of the large density of conduction electrons in metals is a characteristically large and negative dielectric response at low frequencies, increasing with frequency, and crossing over to positive at what is known as the plasma frequency. A typical glass has $\epsilon_b \approx 2.25$ (for a refractive index $n \approx 1.5$) and thus, when the metal's dielectric response reaches $\epsilon_a \approx -4.5$, a resonance absorption occurs. For gold [32], this happens at a photon energy of 2.3 eV (539 nm), resulting in the absorption peak at that energy. Since the frequency where $\epsilon_a = -2\epsilon_b$ depends on the metal, the position of this small particle resonance serves to identify the type of inclusion.

We attempted quantitative fits to the measured absorbance using the Garnett effective medium theory in combination with the known optical response for gold [32], recognizing that the dielectric response for the glass matrix can vary with the type of glass and its constituents. To this end, we approximated the host dielectric response as a wavelength-independent refractive index and allowed it to vary as a fitting parameter. We also attempted to

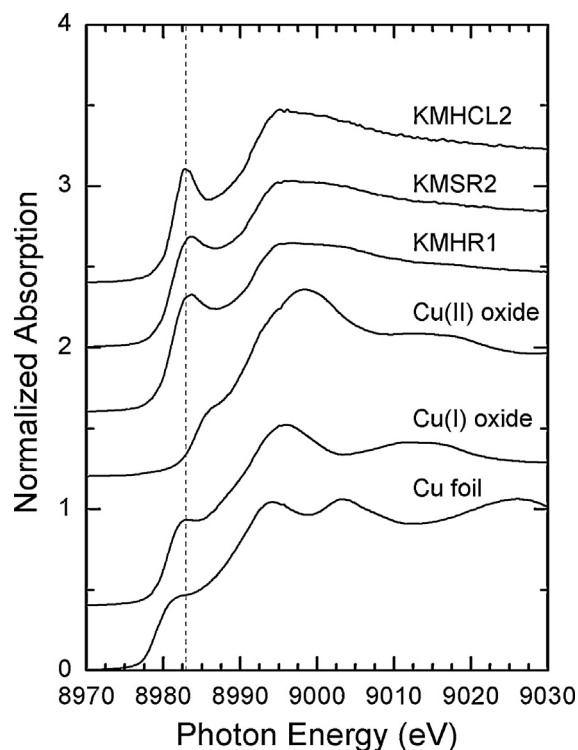


Fig. 5. Cu K-edge XAS spectra of red glasses (KMSR2 and KMHR1), colorless glass (KMHCL2), CuO, Cu₂O and metallic Cu. The spectra are shifted vertically for clarity.

correct the experimental results for losses from the residual paste on the back side by subtracting a constant 0.5 from the absorbance so that it tended toward zero at low photon energies. The optical response for the gold material included a distinct Drude component for describing the conduction electrons. In contrast to electronic interband transitions, the response of the conduction electrons includes a damping factor due to electron scattering. This damping varies with temperature (scattering of electrons from thermally populated lattice vibrations the phonons). It also varies with the particle diameter to account for the scattering of electrons from

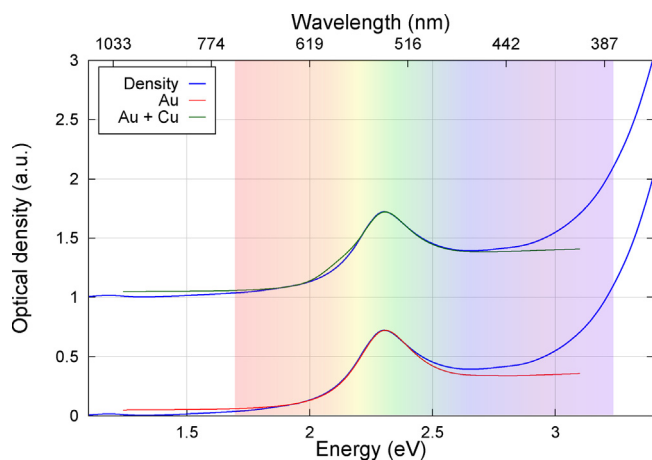


Fig. 6. Optical absorbance spectrum of sample KMHR1. The blue line shows the measured optical absorption spectrum. The lower energy end of the data range was measured with the Si detector while the higher energy end used the GaP detector. The red line shows the result of applying the Garnett theory, as described in the text, to gold particles in glass. The green line, which has been displaced upwards along with a copy of the measured data, shows the result of the Garnett theory for 75% by volume gold particles and 25% copper particles. The background colors denote approximately how the visible spectrum is perceived by the human eye [29].

the particle's surface. The average time between such scattering events can be estimated using the known Fermi velocity of electrons in gold, $v_F = 1.4 \times 10^6$ m/s, as $\tau = r/v_F$ where r is the particle diameter. This gave us three adjustable parameters for fitting with the Garnett theory: the concentration of gold particles, the particle diameter and the refractive index for the glass.

We also considered the possibility that some of the dispersed metallic nanoparticles are copper, which also results [10,24,33] in red coloration in glass and ceramics, although the resonance absorption for Cu is red-shifted compared to Au to 2.18 eV (570 nm). The volume fraction of Cu nanoparticles is a fourth adjustable parameter in the fits using the Garnett theory.

The results for a fit to the absorbance are shown in Fig. 6. As can be seen, the Garnett theory gives a very good fit to the position, strength and width of the absorbance peak near 2.3 eV assuming glass having $n = 1.52$ as the host material, a gold particle volume fraction of 2×10^{-5} , and a particle diameter on the order of 30 nm. However, the fit fails completely for photon energies near and above 3 eV. We suspect this may be from impurities in glass material itself. For example, iron is present (see Fig. 3) in these samples and Fe³⁺ ions result in absorption in the near UV [34]. Arsenic, also present in these samples, is another impurity [35] that could explain the near UV-absorption. Given that the human eye loses sensitivity in the violet and beyond, the red color of these glass tiles can be explained as being predominantly from the small gold particles, which absorb in the green and blue and which allow red light to pass with less attenuation. Subsequent direct measurements of the glass refractive index indicate $n \approx 1.65$, consistent with the known high lead content. The difference from our fit value of $n = 1.52$ may be due to approximations used in developing the Garnett theory, or that the chemical process associated with reducing the precipitating the gold particles leaves each one embedded in a glass shell having smaller n . A 2.7% increase in the gold plasma frequency also remedies the discrepancy.

Given the strong resonance in the measured data at 2.3 eV, it is impossible to fit the optical spectrum with only Cu. The upper plot in Fig. 6 shows the fit using an adjustable fraction of Cu. With 25% Cu by volume, a reasonable fit is found, although with this much Cu, the fitted function deviates from the measurement around the Cu absorption energy of 2.18 eV. While the fit including Cu is closer to the measured spectrum above the Au absorption peak, recall that no effort has been made to model the absorption of these glasses in the ultraviolet, which will certainly result in increasing absorption through the blue, indigo, and violet. We cannot exclude the possibility that some Cu exists in the form of metallic particles in this glass, but the amount relative to Au is certainly *much less* than the 25% considered by the calculation shown in Fig. 6.

5. Discussion

The coloration of the red glass pieces from the 19th century mosaics decorating the exterior of the Temple of the Emerald Buddha is controlled by small, metallic, gold particles dispersed in the glass matrix. XAS data measured at the Au L_{III} edge are consistent with metallic gold. Optical spectroscopy shows that the absorption properties of the glass are consistent with approximately 30 nm diameter gold particles dispersed in the glassy medium. While metallic copper might also contribute to the red coloration, the volume of metallic copper is much smaller than the volume of metallic gold.

Several redox active elements of the sort required for reduction of metallic nanoparticles [10] are present in the glass. Period documentation [5] identifies tin as an ingredient used in glass-making, so it is plausible that it was intentionally added as a reducing agent. We find small quantities of both tin and antimony as well

as a substantial amounts of arsenic and iron. Tin and antimony cannot be seen in Fig. 3 because the incident beam in that figure is below the K-edge energies for those elements. Both are visible when the XRF spectrum is measured with a 31 keV incident beam and both are seen in the chemical analysis shown in Table 2.

The primary source documents [5] refer to both gold and tin – along with other, more cryptic ingredients – as constituents of glass made in Bangkok in the 1830s. Those are the elements that are discussed by Haslbeck et al. [12] for modern recreation of ruby-gold glass. The use of tin or other metals as reducing agents for a noble metal in glass is extensively documented for historical glass-making over centuries and from Europe to Persia [10]. The conjecture that Thai glass-makers of the 1830s intentionally used the ruby-gold technique is well supported both by the material properties of the glass and by the limited historical documentation.

That said, many questions of an art historical nature remain about glass-making in Thailand in the early 19th century. Was ruby-gold glass-making an independently discovered craft or was it imported either from elsewhere in the region or the world? The existing documentation explains nothing about glass blowing and cutting techniques. Finally, little is known about sources of materials for these glasses. Haslbeck et al. [11] report successfully making ruby-gold glass starting from both hydrous chloroauric acid and potassium aurocyanide. In ancient Rome and in early modern Europe, gold was introduced to glass as chloroauric acid formed by dissolution of metallic gold in aqua regia [10]. This is a plausible mechanism for the introduction of gold into the red Kriab glasses.

Acknowledgments

Samples of glass from the Temple of the Emerald Buddha were provided by Thailand's Bureau of the Royal Household under the permission of Her Royal Highness Maha Chakri Sirindhorn. This work was financially supported in part by the Synchrotron Light Research Institute (Public Organization). Use of the National Synchrotron Light Source, Brookhaven National Laboratory, was supported by the U.S. Department of Energy, Office of Science, Office of Basic Energy Sciences, under Contract No. DE-AC02-98CH10886.

References

- [1] S. Diskul, History of the Temple of the Emerald Buddha, Bureau of the Royal Household, Bangkok, Thailand, 1992.
- [2] P. Krairiksh, The Grand Palace and the Temple of the Emerald Buddha: a handbook for guides, Bureau of the Royal Household, Bangkok, Thailand, 1988, pp. 1988.
- [3] W. Klysubun, B. Ravel, P. Klysubun, P. Sombunchoo, W. Deenan, Characterization of yellow and colorless decorative glasses from the Temple of the Emerald Buddha, Bangkok, Thailand, Appl. Phys. A (2013) 1–8.
- [4] P. Sriviboon, Personal communication, Museum and Office of the Temple of the Emerald Buddha, Bangkok, Thailand, 2012, pp. 2012.
- [5] National Library of Thailand. Miscellaneous textbooks, glass melting textbook, call numbers 53, 54, 62, 63, 165 and 167, Undated.
- [6] K. Pongchan, Personal communication, 2014.
- [7] J.C.M. Garnett, Colours in metal glasses and in metallic films, Proc. R. Soc. Lond. 73 (488–496) (1904) 443–445.
- [8] J.C.M. Garnett, Colours in metal glasses, in metallic films and in metallic solutions II, Proc. R. Soc. Lond. A Math. Phys. Sci. (1905) 370–373.
- [9] F.E. Wagner, S. Haslbeck, L. Stievano, S. Calogero, Q.A. Pankhurst, K.-P. Martinek, Before striking gold in gold-ruby glass, Nature 407 (6805) (2000) 691–692.
- [10] P. Colomban, The use of metal nanoparticles to produce yellow, red and iridescent colour, from bronze age to present times in lustre pottery and glass: solid state chemistry, spectroscopy and nanostructure, J. Nano Res. 8 (2009) 109–132, <http://dx.doi.org/10.4028/www.scientific.net/JNanoR.8.109>.
- [11] R. Wilson, The use of gold nanoparticles in diagnostics and detection, Chem. Soc. Rev. 37 (9) (2008) 2028–2045.
- [12] S. Haslbeck, K.-P. Martinek, L. Stievano, F. Wagner, Formation of gold nanoparticles in gold-ruby glass: the influence of tin, in: P.-E. Lippens, J.-C. Jumas, J.-M. Génin (Eds.), ICAME 2005, Springer, Berlin Heidelberg, 2007, pp. 89–94 (ISBN 978-3-540-49848-3).
- [13] K. Won-in, Y. Thongkam, S. Pongkrapan, S. Intarasiri, C. Thongleurm, T. Kamwanna, T. Leelawathanasuk, P. Dararutana, Raman spectroscopic study on archaeological glasses in Thailand: ancient Thai Glass, Spectrochim. Acta A Mol. Biomol. Spectros. 83 (1) (2011) 231–235.
- [14] J. Golovchenko, R. Levesque, P. Cowan, X-ray monochromator system for use with synchrotron radiation sources, Rev. Sci. Instrum. 52 (4) (1981) 509–516.
- [15] B. Ravel, C. Scorzato, D.P. Siddons, S.D. Kelly, S.R. Bare, Simultaneous XAFS measurements of multiple samples, J. Synchrotron Radiat. 17 (3) (2010) 380–385.
- [16] B. Ravel, M. Newville, ATHENA, ARTEMIS, HEPHAESTUS: data analysis for X-ray absorption spectroscopy using IFEFIT, J. Synchrotron Radiat. 12 (4) (2005) 537–541.
- [17] W. Klysubun, P. Sombunchoo, W. Deenan, C. Kongmark, Performance and status of beamline BL8 at SLRI for X-ray absorption spectroscopy, J. Synchrotron Radiat. 19 (6) (2012) 930–936.
- [18] R. Wolf, S. Wilson, U.S. Geological Survey Fact Sheet 2007-3056, USGS Reference Materials Program, USGS, 2007.
- [19] N.J. Pearce, W.T. Perkins, J.A. Westgate, M.P. Gorton, S.E. Jackson, C.R. Neal, S.P. Chenery, A compilation of new and published major and trace element data for NIST SRM 610 and NIST SRM 612 glass reference materials, Geostand. Newsl. 21 (1) (1997) 115–144.
- [20] K.P. Jochum, M. Willbold, I. Raczek, B. Stoll, K. Herwig, Chemical Characterisation of the USGS Reference Glasses GSA-1G, GSC-1G, GSD-1G, GSE-1G, BCR-2G, BHVO-2G and BIR-1G Using EPMA, ID-TIMS, ID-ICP-MS and LA-ICP-MS, Geostand. Geoanal. Res. 29 (3) (2005) 285–302.
- [21] B. Mandal, K. Suzuki, Arsenic round the world: a review, Talanta 58 (1) (2002) 201–235.
- [22] J.C. Woicik, B. Ravel, D.A. Fischer, W.J. Newburgh, Performance of a four-element Si-drift detector for X-ray absorption fine-structure spectroscopy: resolution, maximum count rate, and dead time correction with incorporation into the ATHENA data analysis software, J. Synchrotron Radiat. 17 (3) (2010) 409–413.
- [23] R.E. Benfield, D. Grandjean, M. Kröll, R. Pugin, T. Sawitowski, G. Schmid, Structure and Bonding of Gold Metal Clusters, Colloids, and Nanowires Studied by EXAFS, XANES, and WAXS, J. Phys. Chem. B 105 (10) (2001) 1961–1970.
- [24] W. Klysubun, Y. Thongkam, S. Pongkrapan, K. Won-in, J. T-Thienprasert, P. Dararutana, XAS study on copper red in ancient glass beads from Thailand, Anal. Bioanal. Chem. 399 (9) (2011) 3033–3040.
- [25] F. Farges, M.-P. Etcheverry, A. Scheidegger, D. Grolimund, Speciation and weathering of copper in copper red ruby medieval flashed glasses from the Tours cathedral (XIII century), Appl. Geochem. 21 (10) (2006) 1715–1731.
- [26] F.A. Kirkpatrick, G.G. Roberts, Production of selenium red glass, J. Am. Ceramic Soc. 2 (11) (1919) 895–904, <http://dx.doi.org/10.1111/j.1151-2916.1919.tb18751.x> [ISSN 1551-2916].
- [27] K. Nassau, The physics and chemistry of color, the fifteen causes of color, 2nd edn., Wiley-Interscience, 2001.
- [28] C. Maurizio, F. d'Acapito, M. Benfatto, S. Mobilio, E. Cattaruzza, F. Gonella, Local coordination geometry around Cu⁺ and Cu²⁺ ions in silicate glasses: an X-ray absorption near edge structure investigation, Eur. Phys. J. B, Condensed Matter Complex Syst. 14 (2) (2000) 211–216.
- [29] T.J. Bruno, P.D.N. Svoronos, CRC handbook of fundamental spectroscopic correlation charts, CRC Press, 2005.
- [30] O. Yeshchenko, I. Bondarchuk, V. Gurin, I. Dmitruk, A. Kotko, Temperature dependence of the surface plasmon resonance in gold nanoparticles, Surf. Sci. 608 (2013) 275–281.
- [31] G.L. Carr, S. Perkowitz, D.B. Tanner, Far-infrared properties of inhomogeneous materials, Infrared Millimeter Waves 13 (1985) 171–263.
- [32] P.B. Johnson, R.W. Christy, Optical constants of the noble metals, Phys. Rev. B 6 (1972) 4370–4379.
- [33] I. Nakai, C. Numako, H. Hosono, K. Yamasaki, Origin of the red color of Satsuma copper-ruby glass as determined by EXAFS and optical absorption spectroscopy, J. Am. Ceramic Soc. 82 (3) (1999) 689–695, <http://dx.doi.org/10.1111/j.1151-2916.1999.tb01818.x> [ISSN 1551-2916].
- [34] D. Ehr, UV-absorption and radiation effects in different glasses doped with iron and tin in the ppm range, C. R. Chim. 5 (11) (2002) 679–692.
- [35] C. Stålhandske, The impact of refining agents on glass colour, Glasteknisk Tidsskrift 55 (3) (2000) 65–71.